Silicon (2023) 15:839–853
https://doi.org/10.1007/s12633-022-02049-z

ORIGINAL PAPER

The Effect of Temperature on Synthetic Nano β-Eucryptite and Alumina Ceramic Materials: Thermal Expansion, Mechanical, and Physical Properties

H. H. Abo-almaged[1] · W. H. Hegazy[2] · M. E. M. Sebak[3] · R. M. Khattab[1]

Received: 10 May 2022 / Accepted: 28 July 2022 / Published online: 15 August 2022

Abstract
The capability to fabricate ultra-low and customizable CTE materials with good mechanical properties in a simple method was demonstrated in this work. For this purpose, nano beta-eucryptite and alumina powders were synthesized and used in the composite's fabrication. Four composites of alumina and a second-phase beta-eucryptite were prepared, containing 10, 20, 30, and 40 wt.% beta-eucryptite. The temperature effect on prepared composites is investigated. The results of XRD analysis and the microstructures of prepared composites are discussed with results of mechanical strength and thermal expansion at temperature ranges of 1400, 1500, and 1550 °C. The CTE of alumina-beta-eucryptite composites decrease as the beta-eucryptite content increases, reaching -1.036 × 10^{-6} °C^{-1}. The findings show that a composite with a very low thermal expansion coefficient and good mechanical properties can be designed and used in different applications.

Keywords Al_2O_3 · Beta-eucryptite · Composite · Thermal expansion · Mechanical properties

1 Introduction

Low coefficient of thermal expansion (CTE) materials is getting a lot of attention due to their wide variety of applications, which range from cookware to aerospace [1].

The first glass ceramics fabricated were ceramic composites based on $Li_2O.Al_2O_3.SiO_2$ (LAS), which have grown in economic and industrial significance. The predominant crystalline phases in these systems are metastable solid solutions with beta-quartz or keatite structures. The lithium ions fill the structure's cavities, providing charge neutrality. The three most important crystalline phases in this system are beta-petalite ($Li_2O.Al_2O_3.8SiO_2$), beta-eucryptite ($Li_2O.Al_2O_3.2SiO_2$), and beta-spodumene ($Li_2O.Al_2O_3.4SiO_2$). The low negative coefficients of thermal expansion of these phases (ranging from 86 × 10^{-7} °C^{-1} for beta-eucryptite to 9 × 10^{-7} °C^{-1} for beta-spodumene) facilitate the production of glass ceramics with dimensional stability and high thermal shock resistance [2–6].

Alumina is one of the most appealing ceramic alternatives due to its high melting point and strong mechanical properties. For example, it has high compressive strength, high hardness, high elastic modulus, and good chemical and thermal stability. However, alumina's low fracture toughness is one of its disadvantages, which may limit its employment in high-mechanical applications. This is attributable to the easiness with which cracks propagate in alumina ceramics. Incorporating a second phase that interacts with alumina boundaries is one method of increasing fracture toughness. Materials with two crystalline phases, for example, could have higher fracture toughness, which improves wear resistance. With alumina ceramics, eucryptite has been employed as a second phase [7–13].

For decades, eucryptite ($Li_2O.Al_2O_3.2SiO_2$) has been widely employed as a Lithia carrying flux and low expansion filler in whiter ware bodies in the glass and ceramics industries. Because of its very-low thermal expansion, high thermal stability, superior thermal shock resistance, and high chemical stability, eucryptite is utilized as a structural material. They are commonly employed in industrial furnaces as

✉ H. H. Abo-almaged
hanan-202@hotmail.com

[1] Refractories, Ceramics and Building Materials Department, National Research Centre (NRC), Dokki 12622, Cairo, Egypt

[2] Department of Chemistry, Faculty of Science, Suez University, Suez 43533, Egypt

[3] Petroleum Medical Centre, Suez, Egypt

refractory materials and as heat exchangers in gas turbines [13–17].

In this study, we will focus on the production of an alumina- eucryptite ceramic composite using the Pechini method. The Pechini method is extensively used for the synthesis of ceramics and composites. This procedure is successful in the synthesis of ceramic powders because it works at low temperatures and achieves good uniformity in the solution phase and gels. The process allows the preparation of ceramic powders with good sinterability, stoichiometry control, and good management of the morphology of particles and agglomerates. The synthesis of lithium aluminosilicate gels utilizing various metal alkoxide starting materials has been extensively studied. Metal alkoxides, which are used as sol–gel synthesis precursors, are extremely costly. The Pechini method now uses inorganic salts due to the time-consuming laboratory synthesis of metal alkoxides, their high cost, and commercial unavailability. Therefore, the second goal of this work is to prepare these composites using chemically pure materials and characterize their phase composition, microstructure, mechanical, and physical properties.

2 Materials and Experimental Procedures

2.1 Starting Materials

Lithium nitrate $LiNO_3$ (PubChem, 99%), aluminum chloride hexahydrate $AlCl_3.6H_2O$ (Alfa Aesar, 98%), ethylene glycol (SDFCL, 99%), citric acid (Sigma-Aldrich, 99.5%), and tetraethyl orthosilicate TEOS (Alfa Asear, 98%) were employed as starting materials in this study.

2.2 Polymeric Precursor

2.2.1 Preparation of Beta-Eucryptite

The method devised by Pechini involves the complexing of cations in an aqueous organic medium and the utilization of low cost chemical precursors. A homogenous ion distribution is also obtained at the molecular level. It works on the principle that certain-hydroxy carboxylic organic acids can form stable chelates with a variety of cations. After adding a poly hydroxylic alcohol to this mixture, the chelate is transformed into a polymer with a uniform distribution of cations. At temperatures as low as 300 °C, the organic component is removed, leaving reactive oxides.

The Pechini method was employed to prepare beta-eucryptite, which has previously been used to synthesize poly cationic powders. The process is based on metallic citrate polymerization with ethylene glycol. A hydro carboxylic acid (citric acid) was utilized in an aqueous medium to chelate cations. When a poly alcohol, such as ethylene glycol, is added, an organic ester is formed, and polymerization is facilitated by heating, resulting in a homogenous form. Metal ions are dispersed equally throughout the organic matrix [18].

At 60–70 °C, 30 gm of citric acid was added with continuous agitation, followed by the addition of 38.6 gm of aluminum chloride hexahydrate ($AlCl_3.6H_2O$) as the polymeric former, (11.032 gm) lithium nitrate ($LiNO_3$), and (33.30 gm) tetraethyl orthosilicate (TEOS) were mixed in a stoichiometric ratio with continuous stirring to get beta-eucryptite. After completely dissolving the salts, 20 gm of ethylene glycol was added to the solution. To speed up the reaction, the citric acid-ethylene glycol mass ratio was set to 60:40%, the temperature was raised to 110–210 °C, and a polymeric gel was generated at the end of the reaction.

2.2.2 Preparation of Nano Alumina

For nano alumina preparation, the same procedure is carried out with utilizing $AlCl_3.6H_2O$ as alumina source.

The resulting gel was heat treated for 1 h at 600 °C to partially decompose the polymeric gel. The obtained materials were deagglomerated in porcelain and passed through a 100 mesh sieve. The powders were fired at temperatures ranging from 600 °C to 1200 °C at a heating rate of 10 °C/min for 1 h to follow the phase compositions.

We used the prepared alumina and beta-eucryptite after calcinations at 1200 °C in this study. Four composites of alumina and a second-phase beta-eucryptite were prepared, containing 10, 20, 30, and 40 wt.% beta-eucryptite and designated as AE1, AE2, AE3, and AE4 respectively. The samples were pressed at 100 MPa and fired at a temperature range of 1400, 1500, and 1550 °C for 2 h.

2.3 Characterization

X-ray diffraction analysis (XRD) was done on the prepared powders fired at 600, 800, 1000, and 1200 °C using Bruker D8 equipment with Cu Kα radiation at a scanning rate of 1 degree per minute. The particle size and morphology of the prepared powder calcined at 1200 °C were characterized using a transmission electron microscopy (TEM, JEOL JEM-1230). The microstructure of the sintered samples was examined using a scanning electron microscope (SEM-Philips XL 30). The Archimedes method was used to measure the apparent porosity and bulk density of the different samples. The coefficient of thermal expansion was measured from 25 to 700 °C at a heating rate of 10 °C min^{-1}. An automatic hydraulic testing machine (Shimadzu Co., Kyoto, Japan) with a maximum capacity of 1,000 KN was used to test the compressive strength of sintered bodies.

3 Results and Discussion

3.1 X-ray Diffraction of Calcined Powders

The XRD patterns of beta-eucryptite and alumina powders at different calcined temperatures are shown in Figs. 1 and 2.

When the gel powders of all prepared samples were calcined at 600 °C for 2 h, the amorphous structure was preserved. In Fig. 1, XRD peaks of the beta-eucryptite phase were detected when the samples were calcined at 800 °C to 1200 °C. With increasing calcination temperatures, the XRD peaks' intensity increased. This shows how heat treatment causes crystallinity to grow in powders. The XRD patterns for the prepared alumina powders demonstrate the development of boehmite (AlOOH) (Fig. 2), which transforms into gamma alumina (γ-Al_2O_3) after calcination at 600, 800, and 1000 °C. Other previous studies have shown that increasing the calcination temperature causes a series of transformations: AlOOH → γ-Al_2O_3 → δ-Al_2O_3 → θ-Al_2O_3 → α-Al_2O [19]. At high temperatures (1200 °C), some of the gamma alumina phases that formed at low temperatures changed to α-Al_2O_3. Low activation energies are required for transitions from γ phase ended to θ phase, while α transformation proceeds occur via nucleation, growth, and higher temperature [20]. At low temperatures, alumina appeared in an amorphous state, which changed to a crystalline state over 1000 °C [21].

3.2 TEM Micrographs

Figure 3 shows TEM images of samples that had been annealed at 1200 °C. The particles are uniform in size and shape, with an average size of 5–50 nm for beta-eucryptite. For beta-eucryptite, the particle size was observed to be on the nanometer scale. On the contrary, alumina appears in hexagonal form with large sizes between 100 and 500 nm. The EDS analysis indicates that the well crystallite for both powders is at 1200 °C.

3.3 SEM Images

SEM of fired powders at 800 °C and 1200 °C is demonstrated in Figs. 4 and 5. Beta-eucryptite particles of small size and irregular forms have been observed. It appeared as dark grey particles that fused together to form a tridimensional structure. Beta-eucryptite is uniformly dispersed in the matrix, with an average particle size varying from 17–25 nm (Fig. 4). At high temperatures, the final structure of eucryptite particles can be related to the big microscopic

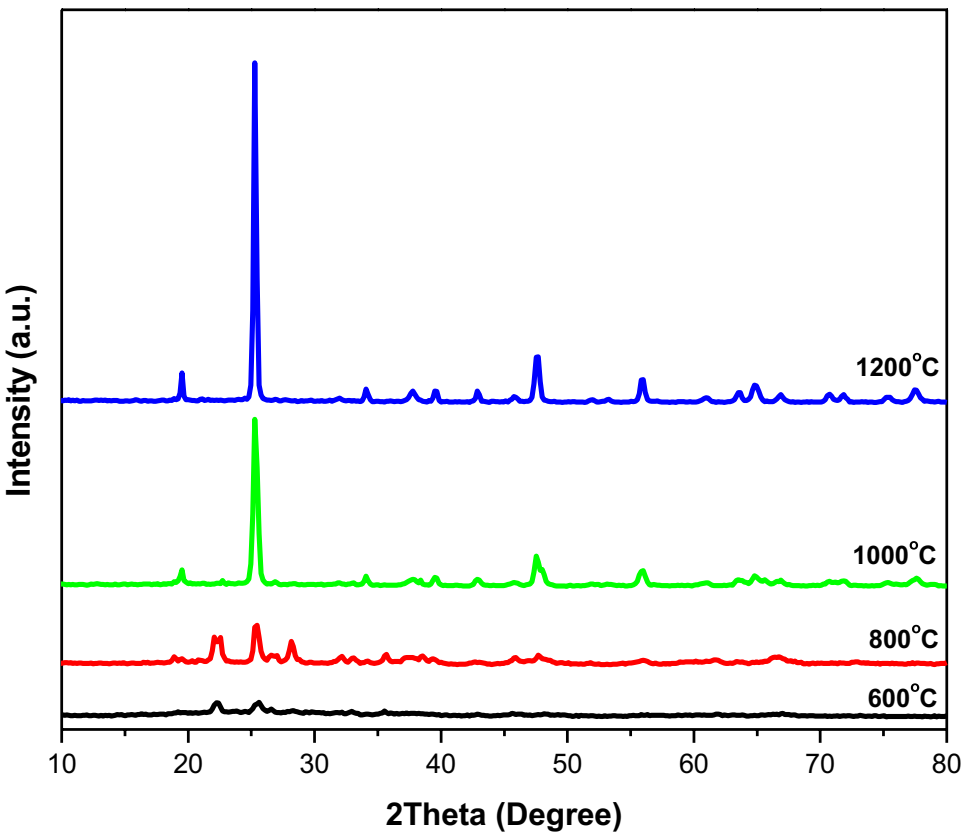

Fig. 1 XRD patterns of beta-eucryptite calcined at different temperatures

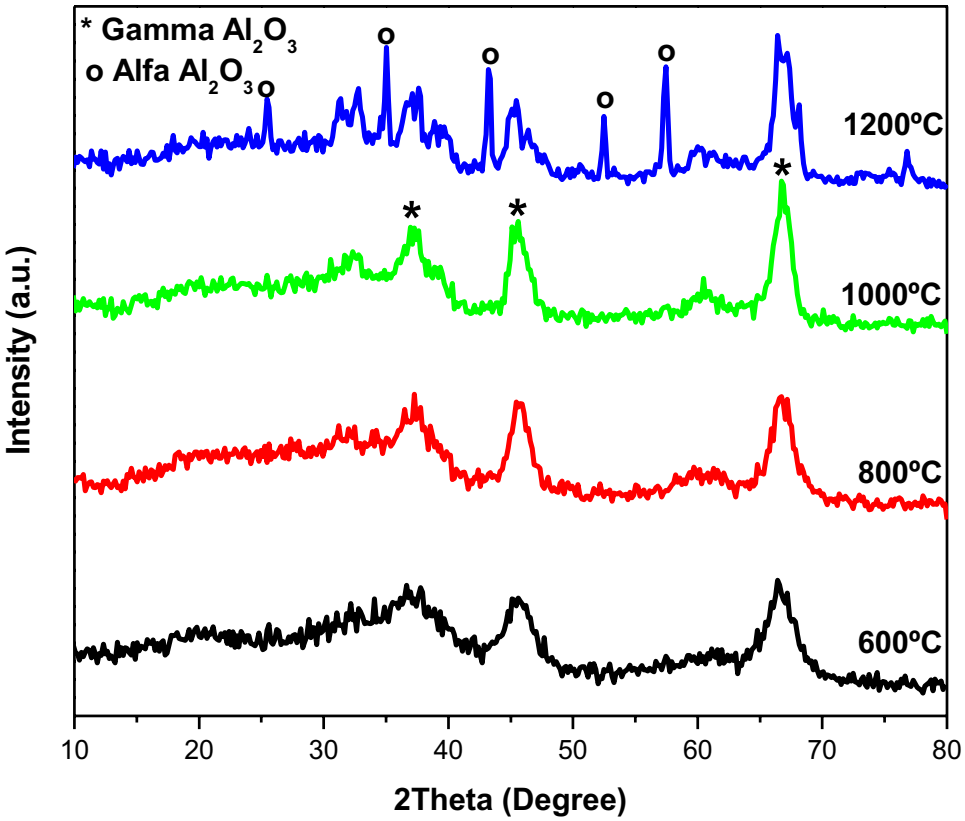

Fig. 2 XRD patterns of alumina calcined at different temperatures

air gas that exists between the particles, resulting in a reduced diffusion rate that inhibits particle growth (Fig. 5). On the other hand, scanning electron microscope for alumina powders fired at various temperatures; 800 °C and 1200 °C are shown in Figs. 4 and 5.

The change in morphology and the size of the powders after calcinations are observed with increasing the firing temperature. For powders fired at low temperatures (800 °C), the aggregation of nano particles into micro particles was observed to be referred to δ-Al_2O_3. For the alumina powder fired at 1200 °C, plate α-alumina was found in the matrix. The α-alumina particles have a size greater than one micron. Plate α-alumina is the main phase for this fired temperature (1200 °C).

3.4 Physical Properties of the Prepared Samples

The bulk density and apparent porosity of beta-eucryptite-alumina composites sintered at 1400, 1500, and 1550 °C with different beta-eucryptite contents (10, 20, 30, and 40 wt.%) are shown in Figs. 6 and 7.

It is widely known that obtaining pore-free sintered beta-eucryptite ($Li_2O.Al_2O_3.2SiO_2$) by the conventional firing process or without the addition of sintering aids during the preparation of beta-eucryptite from micro-sized starting materials is difficult because of the high grain boundary energy of lithium–alumina–silicates that causes the prevailing of grain coarsening [22, 23].

As a result, preparing beta-eucryptite materials at the nano scale may facilitate sintering by reducing pores. Furthermore, in lithium–alumina–silicates (LAS), the Si-rich zone has higher grain boundary mobility than the Al-rich zone. Likewise, magnesium aluminate spinel doped with lithium may help in sintering and grain boundary mobility. According to the figures, increasing the sintering temperature causes an increase in bulk density and a decrease in apparent porosity with increasing beta-eucryptite content up to 1500 °C. This is because when the sintering temperature rises, the solid state reactions between the particles increase. The densification was improved at higher temperatures by the formation of a liquid-phase obtained from the LAS materials. Grain rearrangement, viscous flow, and glass redistribution are thought to be the causes of that behavior up to 1500 °C. Also, it is clear from Figs. 6 and 7 that the bodies always show a decrease in the apparent porosity with increasing sintering temperature and beta-eucryptite content up to 30 wt.% at 1550 °C. Then an increase in apparent porosity and

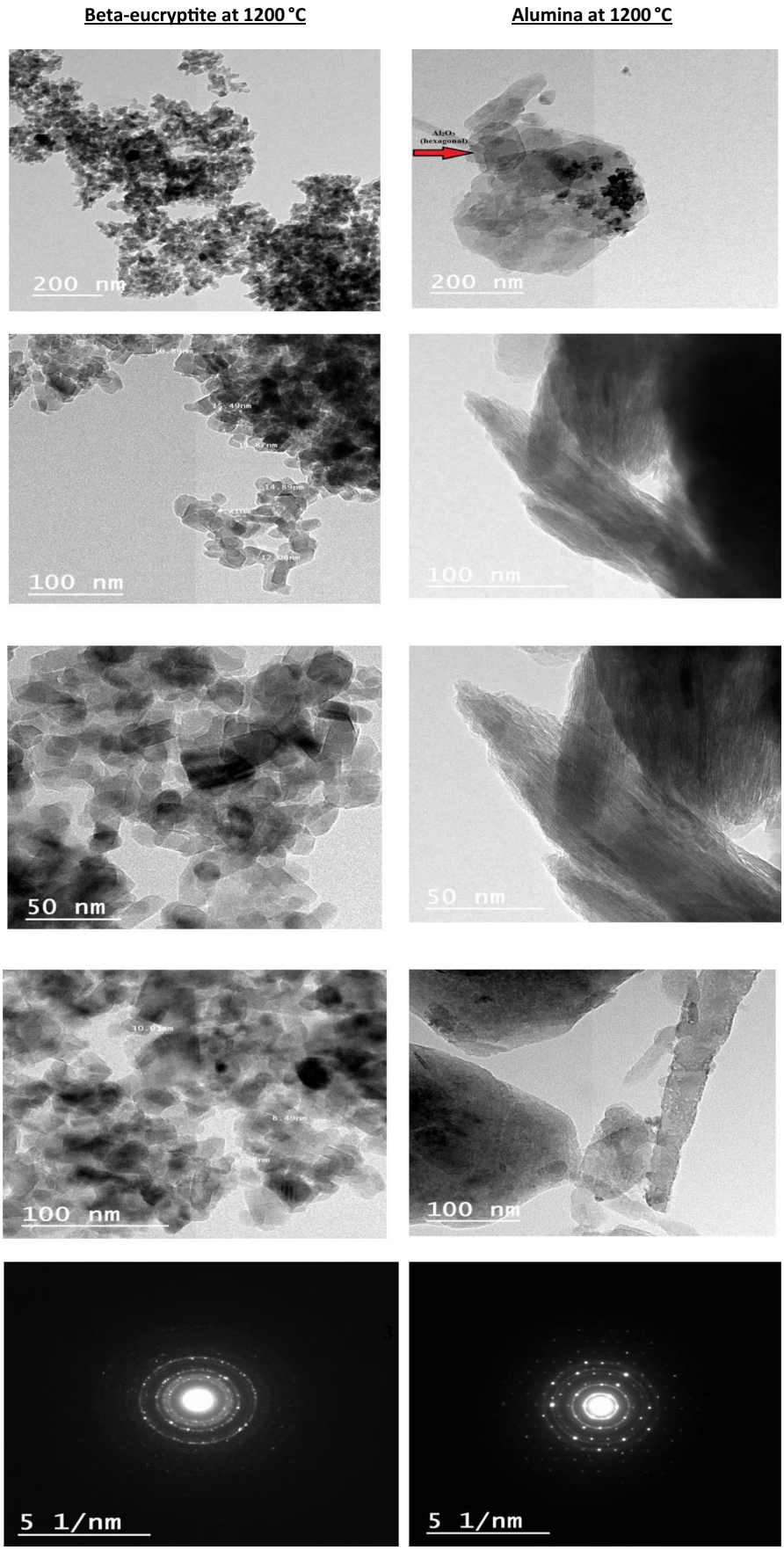

Fig. 3 TEM and EDS analysis of alumina and beta-eucryptite composites sintered at 1200 °C

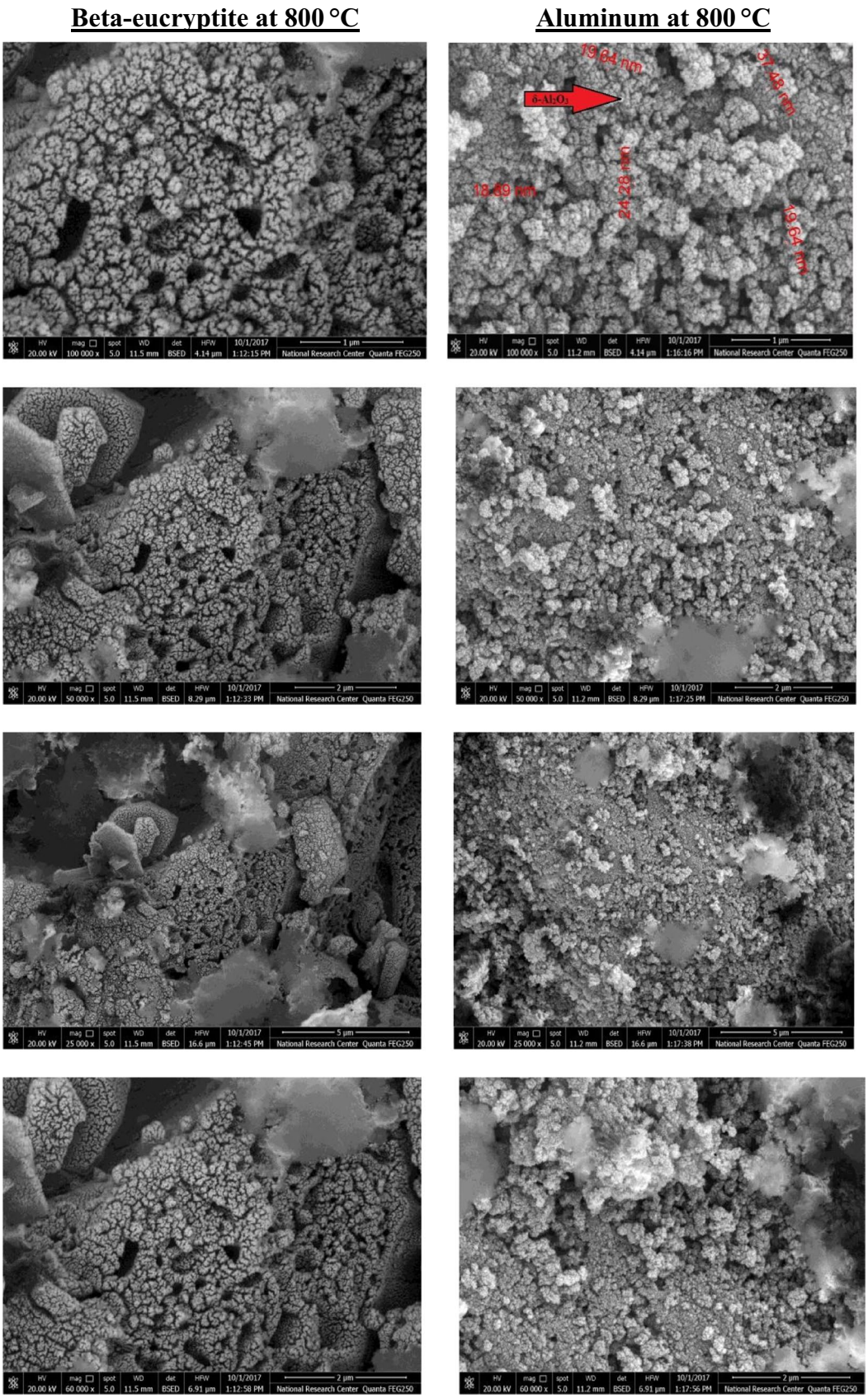

Fig. 4 SEM of calcined alumina and beta-eucryptite composites sintered at 800 °C

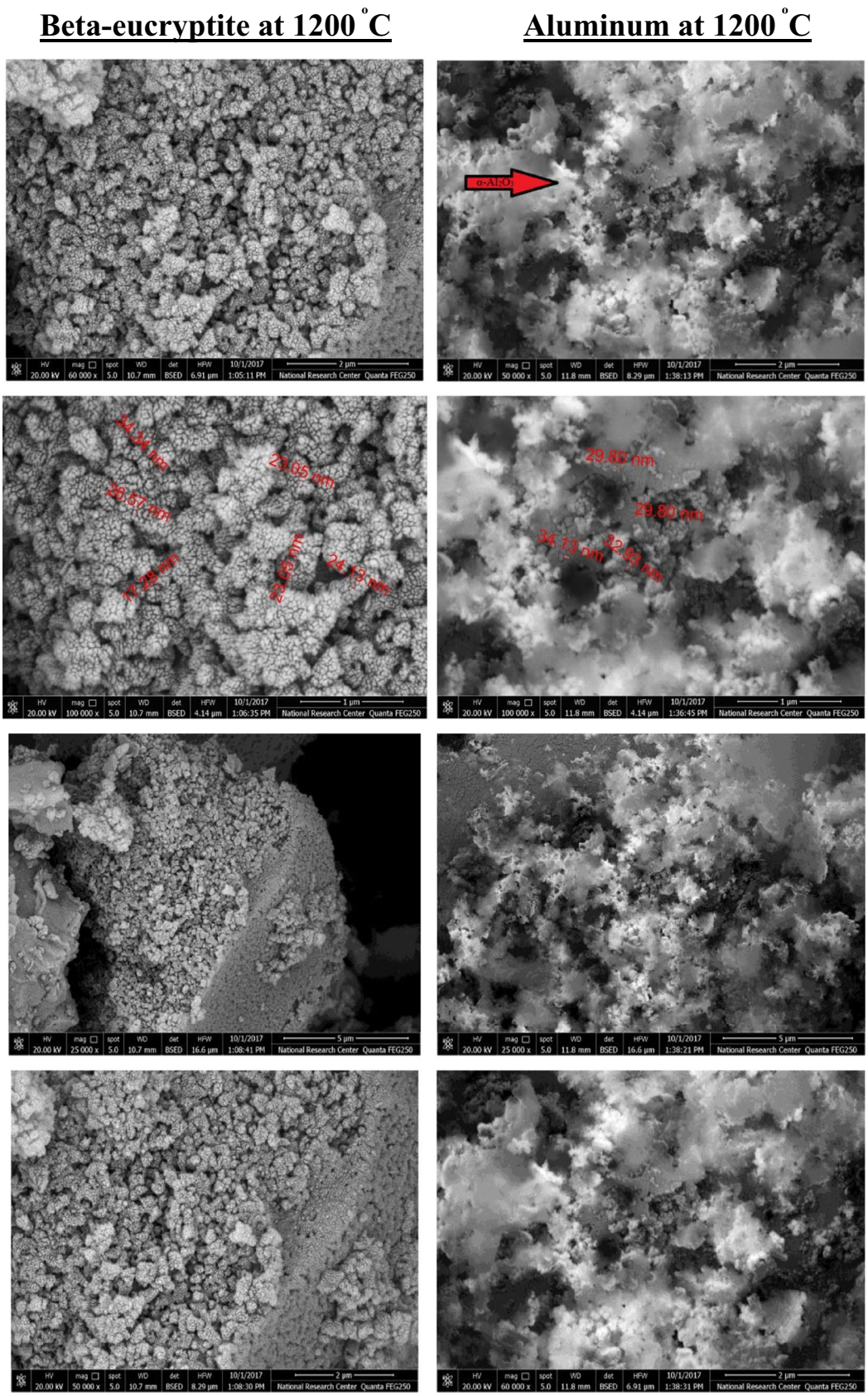

Fig. 5 SEM of calcined alumina and beta-eucryptite composites sintered at 1200 °C

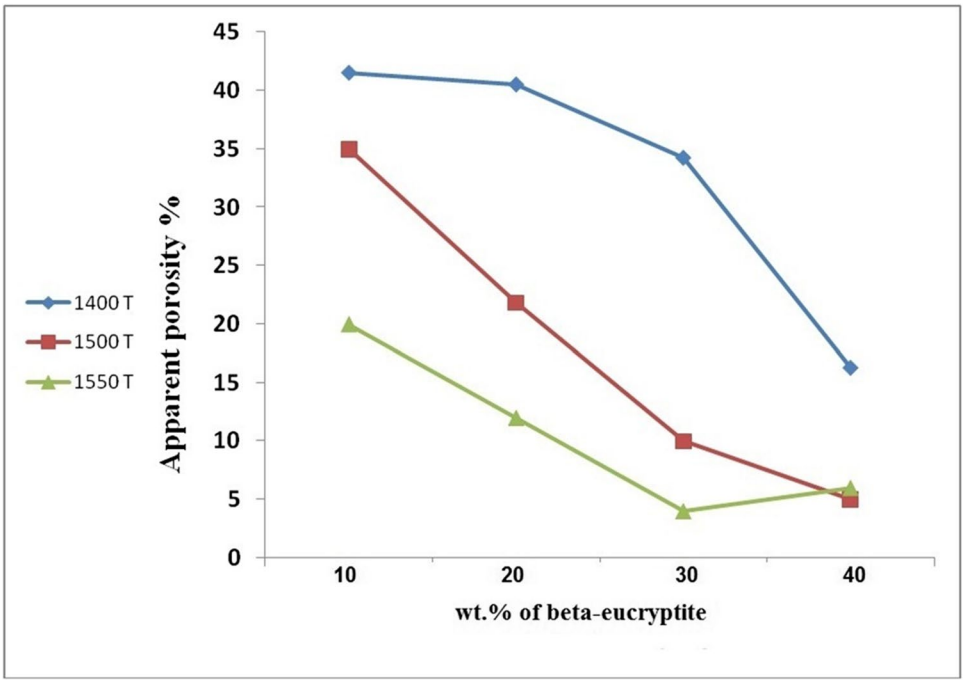

Fig. 6 Apparent porosity of the alumina and beta-eucryptite composites (AE1, AE2, AE3, and AE4) sintered at different temperatures

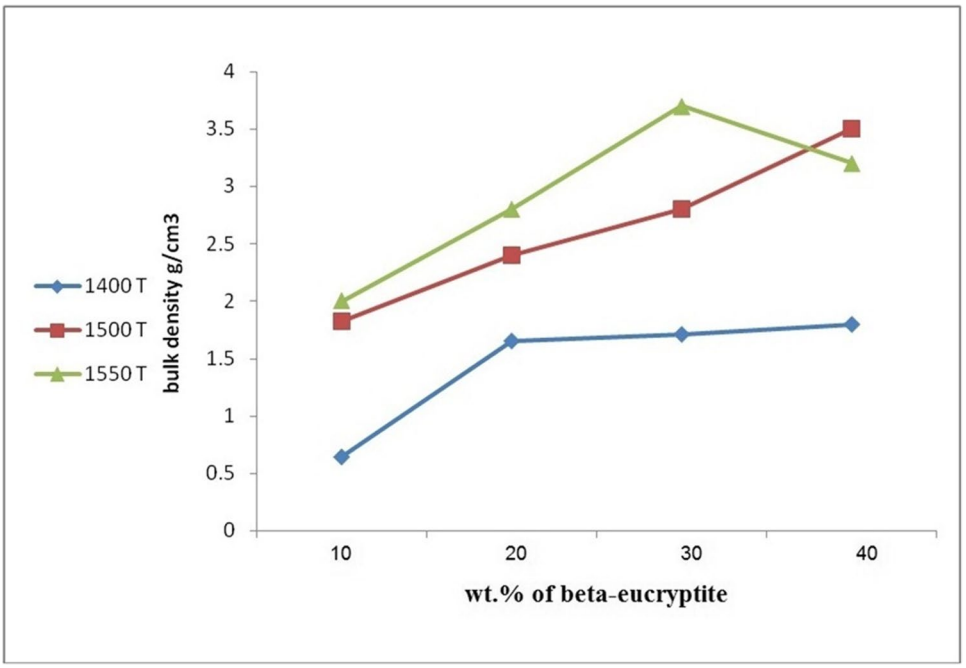

Fig. 7 Bulk density of the alumina and beta-eucryptite composites (AE1, AE2, AE3, and AE4) sintered at different temperatures

a reduction in the bulk density are observed for samples containing 40 wt.%. This result is due to the formation of microcracks and grain growth of beta-eucryptite [6]. In general, the existence of the ternary oxide as the nucleus to obtain the beta-eucryptite grain and the very big alumina grain indicates that the particle size distribution is different (PSD). Such a likely scenario could lead to good densification and a high final relative density [24].

4 XRD Analysis

XRD patterns of alumina-beta-eucryptite composites sintered at different temperatures; 1400, 1500, and 1550 °C are shown in Figs. 8, 9, and 10. It is observed that the beta-eucryptite intensities increase with increasing temperature up to 1500 °C and beta-eucryptite contents. However, increasing the temperatures to 1550 °C increases the

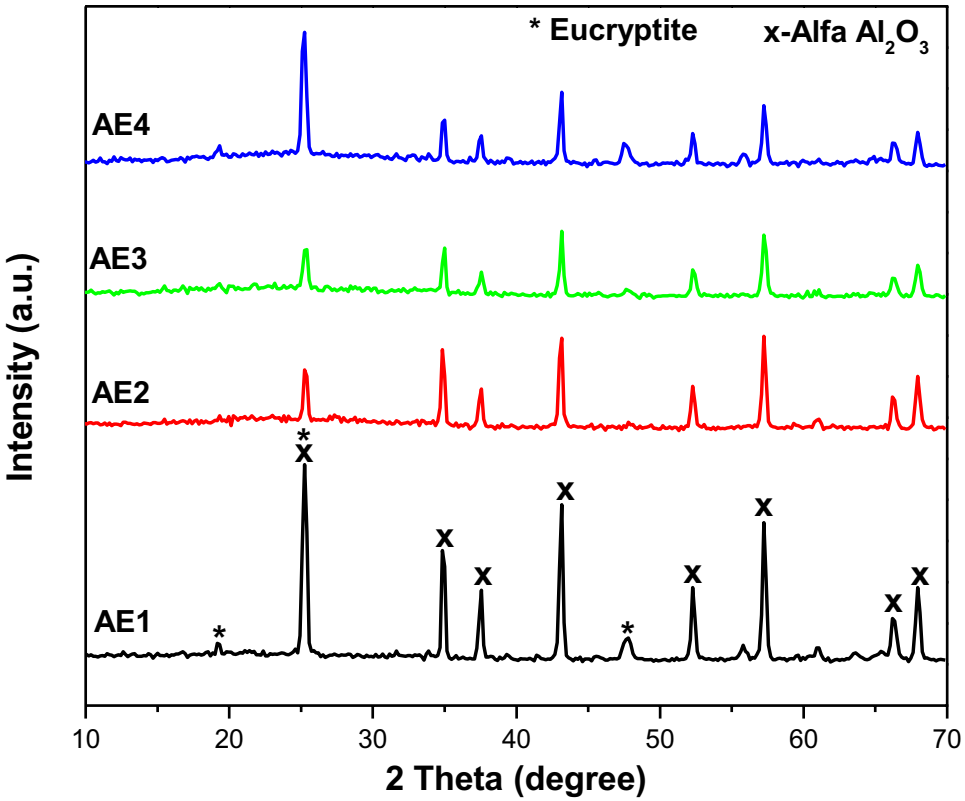

Fig. 8 XRD patterns of the alumina-beta-eucryptite composites AE1, AE2, AE3, and AE4 sintered at 1400 °C

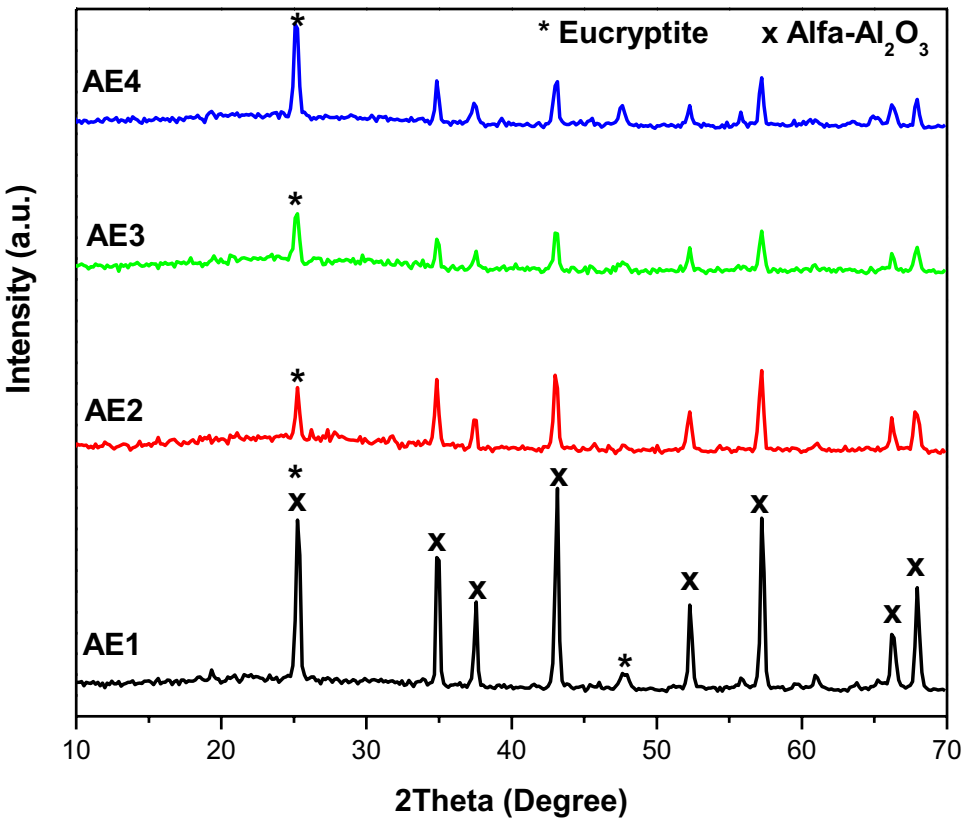

Fig. 9 XRD patterns of the alumina-beta-eucryptite composites AE1, AE2, AE3, and AE4 sintered at 1500 °C

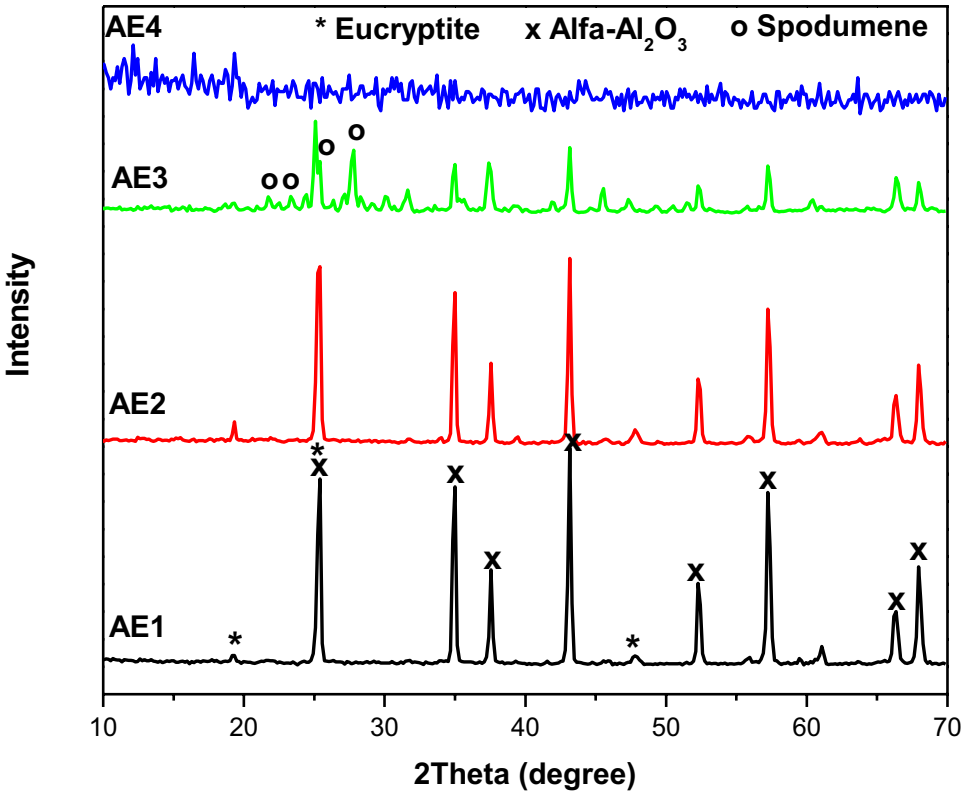

Fig. 10 XRD patterns of the alumina-beta-eucryptite composites AE1, AE2, AE3, and AE4 sintered at 1550 °C

eucryptite contents by up to 30%. In the case of beta-eucryptite 40 wt.% at 1550 °C, the intensity of the peak decreases due to the formation of a high quantity of glassy-phase and the dissociation of some beta-eucryptite into spodumene.

According to the previous work [24, 25], as the heat treatment proceeds, the crystal transforms into a different phase. For example, at high temperatures, crystal-line phases of a eucryptite solid solution convert to the more stable phase of spodumene. The observation of spodumene was observed for samples containing 30 wt.% of beta- eucryptite fired at 1550 °C.

5 SEM Analysis of the Sintered Samples

Microstructure images of alumina containing different amounts of beta-eucryptite and sintered at 1550 °C are shown in Fig. 11 at different magnifications. As seen from these figures, the porosity in most of the samples are appeared for 10, and 20 wt.% beta-eucryptite. The increase in beta-eucryptite content reduces the porosity up to 30 wt.% of beta-eucryptite due to the increase in the glassy phase.

As shown, by increasing the eucryptite content, the alumina plate shape (gray particles) are embedded in a more liquid phase. The highest content of beta-eucryptite (40 wt.%) shows the formation of microcracks (Fig. 11(d)).The presence of microcracking is due to the material's very anisotropic thermal expansion behavior, which produces thermal residual stresses and spontaneous microcracking. Due to the significant anisotropy in the beta-eucryptite crystal structure, which causes the a and b axes to expand while the c axis contracts, microcrack formation is a hallmark feature of beta-eucryptite at high temperatures. Internal stresses are produced when grains break up spontaneously and microcracks form [26, 27]

6 Thermal Expansion Coefficient

The thermal expansion and the coefficient of thermal expansion for different alumina-beta-eucryptite proportions sintered at 1500 °C are shown in Fig. 12 and Table 1, respectively.

In general, since there is no reaction between alumina and the LAS, it is possible to predict the final phase composition and thus design various properties in the material, including its CTE. The CTE value depends on the initial composite composition, resultant body phases, and microstructure. As seen from Table 1, the CTE of alumina-beta-eucryptite composites decreases with increasing the beta-eucryptite content, which was considered a characteristic of beta-eucryptite behavior [6–31]. As it is known, the thermal expansion coefficient of alumina is 10.3×10^{-6} °C^{-1} [32], while beta-eucryptite has a very low thermal expansion coefficient of -6.2×10^{-6} °$C.^{-1}$ [33]

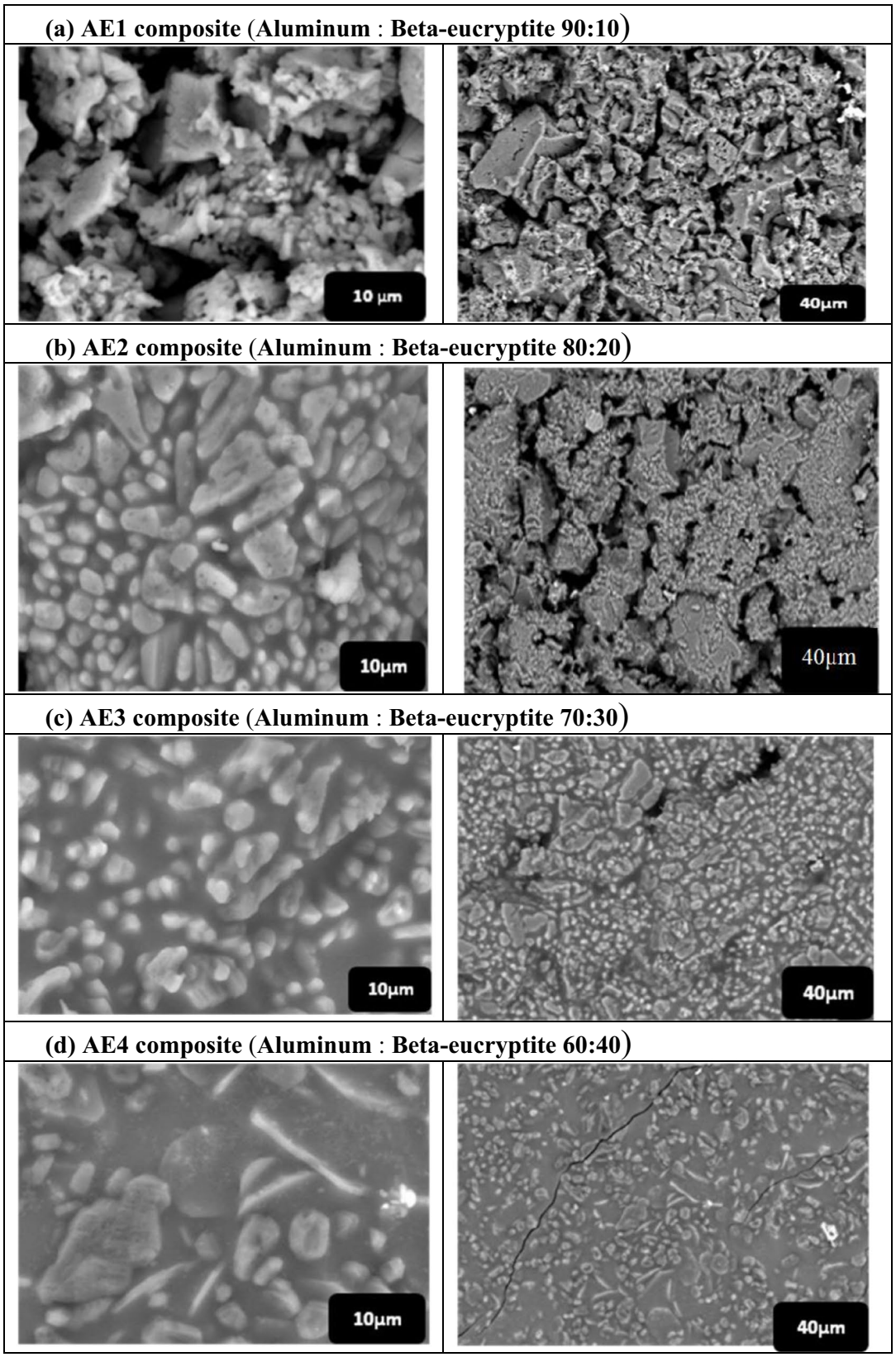

Fig. 11 SEM of the alumina-beta-eucryptite composites: AE1 (**a**), AE2 (**b**), AE3 (**c**), and AE4 (**d**) sintered at 1550 °C

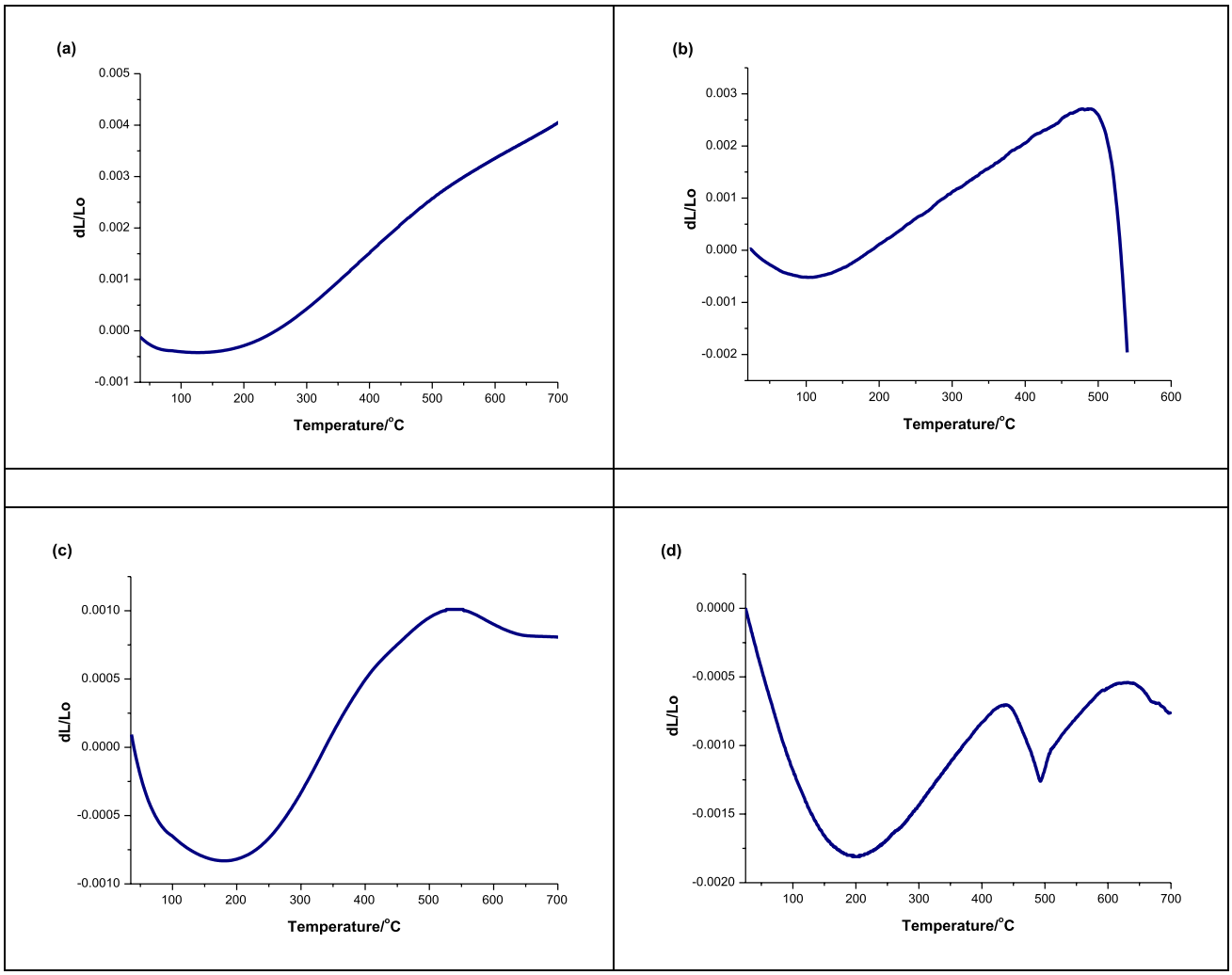

Fig. 12 The thermal expansion of the alumina-beta-eucryptite composites: AE1 (**a**), AE2 (**b**), AE3 (**c**), and AE4 (**d**) sintered at 1500 °C

Table 1 The coefficient of thermal expansion of different alumina-beta- eucryptite proportions sintered at 1500 °C

Composite	Al: Eu	Value of CTE X 10^{-6}/°C
AE1	90: 10	5.77
AE2	80: 20	5.37
AE3	70: 30	1.77
AE4	60: 40	-1.04

7 Mechanical Strength

The mechanical strength of alumina-beta eucryptite composites is shown in Fig. 13. It was observed that samples showed high strength up to 40 wt.% beta-eucryptite content at 1400 °C and 1500 °C, whereas samples with higher beta-eucryptite content (40 wt.%) showed lower strength at 1550 °C. The increase in mechanical strength for samples sintered at 1400 °C and 1500 °C with increasing beta-eucryptite content and at 1550 °C up to 30 wt.% beta-eucryptite is due to the porosity effect [6]. The decrease in mechanical properties of samples containing 40 wt.% beta-eucryptite and sintered at 1550 °C is due to a decrease in density and an increase in porosity as a result of beta-eucryptite grain size enlargement (grain growth) and crack formation.

It is important to note that crack formation has a negative effect on the mechanical properties of fired ceramics [26, 34–40]. For beta-eucryptite, there is a significant thermal expansion anisotropy between the a (8.1×10^{-6} /°C) and c (-17.6×10^{-6} /°C) directions, and due to the large expansion mismatch, spontaneous cracking develops to the extent that extensive crack linking occurs [33]

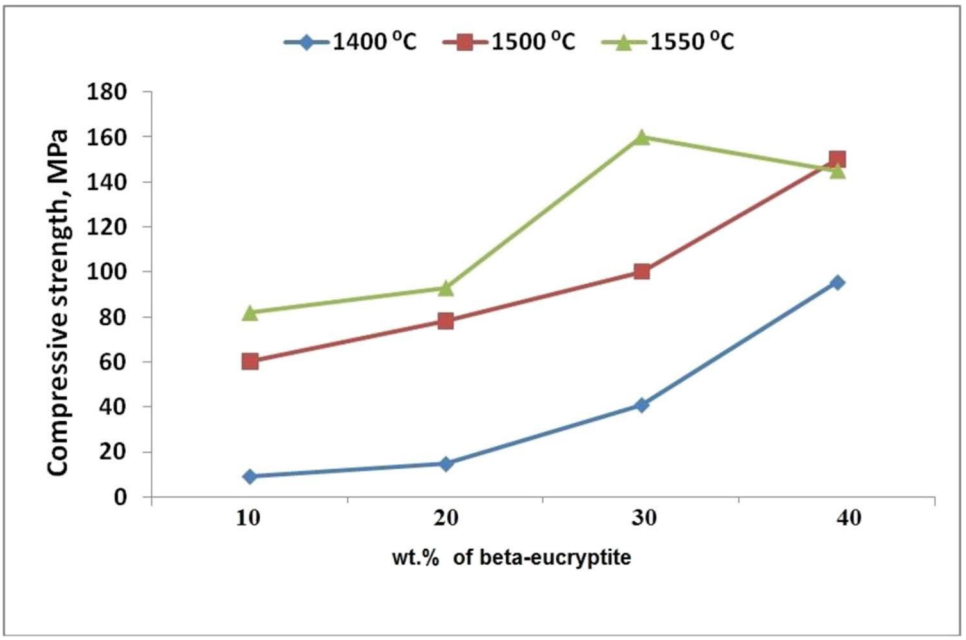

Fig. 13 The mechanical strength of alumina-beta-eucryptite composites (AE1, AE2, AE3, and AE4) sintered at different temperatures

8 Conclusion

The beta-eucryptite-alumina composite presented in this study has demonstrated the capacity to fabricate ultra-low and customized CTE materials with better mechanical properties in a simple and easy manner. In this study, we used the prepared alumina and beta-eucryptite after their calcination at 1200 °C and sintered the prepared composite in a wide temperature range of 1400, 1500, and 1550 °C. The beta-eucryptite is added up to 40 wt.% at the expense of alumina. The results are indicated as follow:

1. Preparing beta-eucryptite materials at the nano scale may facilitate sintering by reducing pores.
2. Increasing the sintering temperature and beta-eucryptite content causes a decrease in apparent porosity up to 1550 °C for a sample containing 30 wt.% of beta-eucryptite.
3. The intensity of crystallizations increases for both phases as the temperature increases to 1550 °C and the beta-eucryptite content increases to 30 wt%.
4. The CTE of alumina-beta-eucryptite composites decreases with increasing beta-eucryptite content to reach -1.036×10^{-6} °C^{-1}.
5. The samples showed a high enhancement of strength up to 30 wt.% of beta-eucryptite.

Authors Contributions All authors contributed to the study conception and design. Material preparation, data collection and analysis were performed by H.H. Abo-almaged, R.M. Khattab, W.H. Hegazy and M.E.M. Sebak. The first draft of the manuscript was written by R.M. Khattab and all authors commented on previous versions of the manuscript. All authors read and approved the final manuscript.

Conceptualization: H.H. Abo-almaged.

Methodology: M.E.M. Sebak.

Formal analysis and investigation: M.E.M. Sebak, H.H. Abo-almaged and R.M. Khattab.

Writing—original draft preparation: R.M. Khattab and M.E.M. Sebak.

Writing—review and editing: H.H. Abo-almaged.

Resources: W.H. Hegazy and M.E.M. Sebak.

Supervision: W.H. Hegazy, R.M. Khattab and H.H. Abo-almaged.

Funding Open access funding provided by The Science, Technology & Innovation Funding Authority (STDF) in cooperation with The Egyptian Knowledge Bank (EKB).

Data Availability Not applicable.

Declarations

Ethics Approval Not applicable: the research did not involve human participants and/or animals.

Consent to Participate All authors have agreed to participate in this research.

Consent for Publication The article was written by the named authors, who are all aware of its content and have given their permission for it to be published.

Competing Interests The authors have no relevant financial or non-financial interests to disclose.

References

1. Garcia-Moreno O, Fernández A, Torrecillas R (2010) Conventional sintering of LAS-SiC nano composites with very low thermal expansion coefficient. J Eur Ceram Soc 30(15):3219–3225
2. M. A. Saleh, S. M. Naga, M. Awaad, A. I. Faid, Y. I. EI- Shaer , Synthesis and characterization of alumina–spodumene ceramic composites, 13th international conference on aerospace sciences & aviation technology, Asat, (2009).
3. Scheidler H, Rodek E (1989) $Li_2OAl_2O_3SiO_2$ glass ceramics. Ceram Bull 68(11):1926–1930
4. Partridge G (1994) An over view of glass ceramics: Part 1 – development and principle bulk applications. Glass Technol 35(3):116–127
5. Sung YM, Dunn SA, Kousky JA (1994) The effect of barium and titania addition on the crystallization and sintering behaviour of $Li_2OAl_2O_3SiO_2$ glass. J Eur Ceram Soc 14:455–462
6. Khattab RM, Sadek HEH, Taha MA, El-Rafei AM (2021) Recycling of silica fume waste in the manufacture of β-eucryptite ceramics. Mater Charact 171:110740
7. Knickerbockers S, Tuzzoloands MR (1989) Lawhone, Sinterable β-spodumene glass ceramics. J Am Ceram Soc 72(10):1873–1379
8. Medvedovski E (2006) Alumina-mullite ceramics for structural applications. Ceram Int 32(4):369–375
9. Hearth GR, Johnson TD, Parry MT, Wall DJ (1990) Solid particle corrosion of alumina lining for pulverized fuel transport piping. Brit Ceram Trans 89:17–21
10. Nicoletto G, Esposito L, Tucci A (1997) Wear and microstructure of poly crystalline alumina. Ceram Acta 9:9–13
11. Medvedovski E (2000) Wear-resistant alumina ceramics. Interceram 49(2):106–133
12. Medvedovski E (2001) Wear-resistant engineering ceramics. Wear. 249(9):821–828
13. Rocha-Rangel E, Refugo-Garcia E, Miranda-Hernandez JG, Terés-Rojas E (2009) Fracture toughness enhancement for material-reinforced alumina. J Cream Process Res 10(6):744–747
14. Wahsh MMS, Khattab RM, Awaad M (2012) Thermo-mechanical properties of mullite/zirconia reinforced alumina ceramics. Mater Des 41:31–36
15 Moustafa EB, Abu Shanab WS, Ghandourah E, Taha MA (2020) Microstructural, mechanical and thermal properties evaluation of AA6061/Al_2O_3-BN hybrid and mono nano composite surface. JMRT 6:15486–15495
16. Ghosh NN, Parmanik P (1997) Synthesis of eucryptite and eucryptite –zirconia composite powders using aqueous sol-gel technique materials. Mater Sci Eng B 49:79–83
17. Yang JS, Sakka S, Yoko T, Kozuka H (1991) Preparation of lithium aluminosilicate glass-ceramic monolith from metal alkoxide solution. J Mater Sci 26:1827–1833
18. Zakia T, Kabelb Khalid I, Hassana H (2012) Using modified Pechini method to synthesize α-Al_2O_3 nanoparticles of high surface area. Ceram Int 28(6):4861–4866
19. Abo-almaged HH, Hegazy WH, Azmy MS, Khattab RM (2021) Extraction of alumina from industrial waste pollutants for the preparation of blue spinel ceramic materials: Processing and characterization. Mater Chem Phys 267:125400
20. Khattab RM, Sadek HEH, Abd-EL-Raoof F, Badra HA, Abo-Almaged HH (2021) Effect of alkali roasting and sulfatization on the extraction of different metal oxides from waste alum sludge. Ceram Int 47:23181–23193
21. Khattab RM, Badr HA, Abo-Almaged HH, Sadek HEH (2018) Recycling of alum sludge for alpha Al_2O_3 production using different chemical treatments. Desalination Water Treat 113:148–159
22. Geodakyan JA, Kostanyan AK, Geodakyan KJ, Sagatelyan ST, Petrosyan BV (2004) The influence of beta-eucryptite glass ceramics on the structure and main properties of alumna ceramic. In: 28th international conference on advanced ceramics and composites:B 37-42
23. Naga SM, El-Maghraby AA, Mörtel H (2006) Densification and characterization of β-spodumene–cordierite compositions. Am Ceram Soc Bull 85(11):9101–9910
24. Jochum T, Reimanis I (2010) Reaction in Eucryptite-Based Lithium Aluminium Silicates. J Am Ceram Soc 93(6):1591–1596
25. Wang MC, Wu NC, Yang S, Wen SB (2003) Morphology and microstructure in the sintering of b-spodumene precursor powders with TiO_2 additive. J Eur Ceram Soc 23:437–443
26. Benavente R, Salvador MD, Martínez-Amesti A, FernAndez A, Borrell A (2016) Effect of sintering technology in β-eucryptite ceramics: influence on fatigue life and effect of microcracks. Mater Sci Eng A 651:668–674
27. Zhao Li-Min, Cheng Yong-Guang, Hao-Shan Hao J, Wang Shao-Hui Liu, Zhang B (2018) Properties of negative thermal expansion b-eucryptite ceramics prepared by spark plasma sintering. Chin Phys B 27(9):096501
28. Mandal S, Chakrabarti S, Das S, Ghatak S (2004) Sintering characteristics of in situ formed low expansion ceramics from a powder precursor in the form of hydroxy hydrogel. Ceram Int 30:2147–2155
29. Benavente R, Borrell A, Salvador MD, Moreno OG, Penaranda-Foix F, Catalá-Civera JM (2014) Fabrication of near-zero thermal expansion of fully dense β-eucryptite ceramics by microwave sintering. Ceram Int 40:935–941
30. Breval E, McKinstry HA, Agrawal DK (2000) New [NZP] materials for protection coatings, Tailoring of thermal expansion. J Mater Sci 35(13):3359–3364
31. Xia L, Wen GW, Song L, Wang XY (2010) The crystallization behavior and thermal expansion properties of b-eucryptite prepared by sol-gel route. Mater Chem Phys 119:495–498

32. Huntz AM, Maréchal L, Lesage B, Molins R (2006) Thermal expansion coefficient of alumina films developed by oxidation of a FeCrAl alloy determined by a deflection technique. Appl Surf Sci 252:7781–7787
33. Pelletant A et al (2012) Grain size dependence of pure β-eucryptite thermal expansion coefficient. Mater Lett 66:68–71
34. Kitouni S, Harabi A (2011) Sintering and mechanical properties of porcelains prepared from algerian raw materials. Ceramica 57:453–460
35. Xia L, Wen G, Liang S, Wang X (2010) The crystallization behavior and thermal expansion properties of β-eucryptite prepared by sol–gel route. Mater Chem Phys 119:495–498
36. Xiao Z, Sun X, Liu K, Luo W, Wang Y, Luo M, Han R, Liu Y (2016) Crystallization behaviors, thermo-physical properties and seal application of Li_2O-ZnO-MgO-SiO_2 glass-ceramics. J Alloys Compd 657:231–236
37. Bruno G, Garlea VO, Muth J, Efremov AM, Watkins TR, Shyam A (2012) Acta Mater 60:4982–4996
38. Arcaroa S, Nietoc MI, Morenoc R, Salvadord MD (2017) LZS/Al_2O_3 glass-ceramic composites sintered by fast firing. Mater Res 20(Suppl. 2):84–91
39. Awaad M, Mortel H, Naga SM (2005) Densification, mechanical and microstructure properties of β-spodumene-alumina composites. J Mater Sci 16(6):377–381
40. Thompson JY, Stoner BR, Piascik JR (2007) Ceramics for restorative dentistry: Critical aspects for fracture and fatigue resistance. Mater Sci Eng 27(3):565–569